RSC Advances

ROYAL SOCIETY OF CHEMISTRY

www.rsc.org/advances

Graphic Abstract for:

Electroluminescence and Fluorescence Response towards Acid Vapors Depending on the Structures of Indole-fused Phospholes

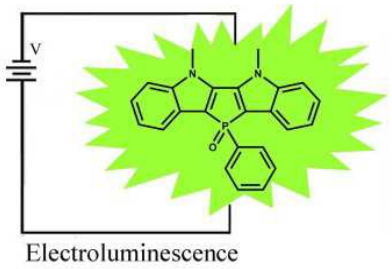

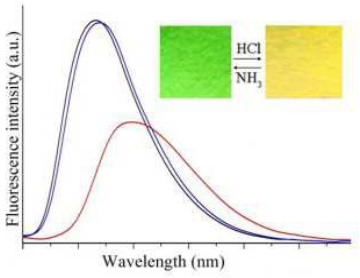

Journal Name

ARTICLE

Electroluminescence and Fluorescence Response towards Acid Vapors Depending on the Structures of Indole-fused Phospholes

Received 00th January 20xx,
Accepted 00th January 20xx

DOI: 10.1039/x0xx00000x

www.rsc.org/

Peng Gong[a], Kaiqi Ye[a,*], Jingbo Sun[a], Peng Chen[b], Pengchong Xue[a], Hao Yang[a] and Ran Lu[a,*]

New isomers of phosphole heteroacenes **2-DIPO** and **3-DIPO**, in which indoles were fused with phospholes in different manners, have been synthesized. It is found that **2-DIPO** containing 5,6-dihydrophospholo[3,2-b:4,5-b']diindole skeleton is high emissive in solution and in solid state, but the emission of **3-DIPO** bearing 5,7-dihydrophospholo[2,3-b:5,4-b']diindole is weak because the emision of **2-DIPO** and **3-DIPO** is originated from π*-π and π*-n transitions, respectively. The OLED using **2-DIPO** as emitter exhibits better performance than that based on **3-DIPO** on account of the poor emission of **3-DIPO**. It is interesting that the filter paper strip containing **2-DIPO** could sense gaseous strong acid by naked eyes. For example, the emitting color of the test paper changes from green to yellow upon exposed to HCl vapor, and can recover upon exposed to gaseous NH_3. This is the first example for the fluorescence sensory probe based on phosphole to detect acid vapors. However, acid cannot induce the change of the emission for **3-DIPO** due to the steric effect of neighboring groups of N-CH_3 and benzene around P=O to prevent the formation of H-bonding between acid and P=O in **3-DIPO**.

Introduction

Organic π-conjugated systems have gained increasing interests from both fundamental and technological viewpoints due to their promising applications in electronic and optoelectronic devices.[1,2] Till now, many fused heterocyclic substructures have been involved in the organic functional materials for tailoring their functionalities.[3-4] In particular, N fused heterocyclic compounds usually exhibit excellent carrier mobility, strong fluorescence emission and good self-assembling properties, so that they have been used as hole transport materials, light harvesting antenna, fluorescence sensors and building blocks in supramolecular assemblies.[5-7] For example, indole derivatives have been designed to show good performance in electrochromic devices (ECDs), organic light-emitting diode (OLED) and anion probing.[8-12] Liu et al synthesized ladder-type diindolo[3,2-b:4,5-b']thiophene, which exhibited low-lying energy level of highest occupied molecular orbital (HOMO) and large band gap, had potential application in organic field effect transistor (OFET).[13] We have synthesized indolocarbazole derivatives, from which emitting nanofibers were generated via organogelation to detect TNT.[6a-b] It is worth noting that the aromatic rings-fused phospholes have received much attention on account of their unique optoelectronic properties, good thermal stability, stability against oxidant and easy structural modification.[14,15] However, to the best of our knowledge, there is no example of bisindole-fused phospholes, although benzothiophene-fused, benzofuran-fused and indole-fused phospholes have been prepared.[16-18] In order to enrich the members of the family of phospholes, which are still reported limitedly, and to reveal their structure-property relationship, we designed two new isomers of indole-fused phospholes **2-DIPO** and **3-DIPO**, in which indoles were fused with phospholes in different manners. It was found that **2-DIPO** containing 5,6-dihydrophospholo[3,2-b:4,5-b']diindole skeleton gave strong emission in solution and in solid state. The OLED using **2-DIPO** as emitter exhibited moderate performance. Notably, the filter paper strip containing **2-DIPO** could sense gaseous strong acid by naked eyes reversibly. This is the first example for the fluorescence sensory material based on phosphole towards acid vapors. Although the emission of **3-DIPO** bearing 5,7-dihydrophospholo[2,3-b:5,4-b']diindol was weak in solution, it was also emissive in solid states. The performance of OLED based on **3-DIPO** was poor due to its low fluorescence quantum yield. Meanwhile, acid vapor could not induce the change of the emission of **3-DIPO** because of the steric effect of the neighboring groups of N-CH_3 and benzene ring around O=P to forbid the formation of H-bonding between acid and O=P in **3-DIPO**. Therefore, the fused manner of indoles to phospholes played a key role on the properties of phosphole derivatives. It provided a strategy for design novel phospholes with desired functionalities.

[a] State Key Laboratory of Supramolecular Structure and Materials, College of Chemistry, Jilin University, Changchun 130012, P. R. China
E-mail: yekq@jlu.edu.cn, luran@mail.jlu.edu.cn
[b] Key Laboratory of Functional Inorganic Material Chemistry (MOE), School of Chemistry and Materials Science, Heilongjiang University, No. 74, Xuefu Road, Nangang District, Harbin, P. R. China

Electronic Supplementary Information (ESI) available: ^{1}H NMR, ^{13}C NMR, ^{31}P NMR and MALDI/TOF MS spectra; CV, DSC and TGA curves; deposition numbers of the single crystals of **2-DIPO** and **3-DIPO** are CCDC 1052683 and CCDC 1042193, respectively. See DOI: 10.1039/x0xx00000x

Results and discussion

Synthesis

The synthetic routes for indole-fused phosphole derivatives **2-DIPO** and **3-DIPO** were shown in Scheme 1. Firstly, 3,3'-dibromo-1,1'-dimethyl-1H,1'H-2,2'-biindole **1** and 1,1'-dimethyl-1H,1'H-3,3'-biindole **2** were synthesized according to the reported literatures.[12,14,19] The ring-forming reaction of compound **1** with DCPP (dichlorophenyl phosphine) catalyzed by *n*-BuLi, followed by the oxidation with H_2O_2 afforded **2-DIPO** in a yield of 60%. The bromination reaction of compound **2** with NBS yielded compound **3**, which could be transformed into **3-DIPO** via similar ring-forming reaction. **2-DIPO** and **3-DIPO** were characterized by ^{1}H NMR, ^{13}C NMR, ^{31}P NMR, FT-IR and MALDI/TOF MS (Figures S13-S21). In ^{31}P NMR spectra, the chemical shifts of phosphorus in **2-DIPO** and **3-DIPO** appeared at 9.00 ppm and 6.79 ppm, respectively, indicating higher density of electron cloud around phosphorus in **3-DIPO** than in **2-DIPO** since two nitrogen atoms were located at α-positions of phosphole ring in **3-DIPO**.

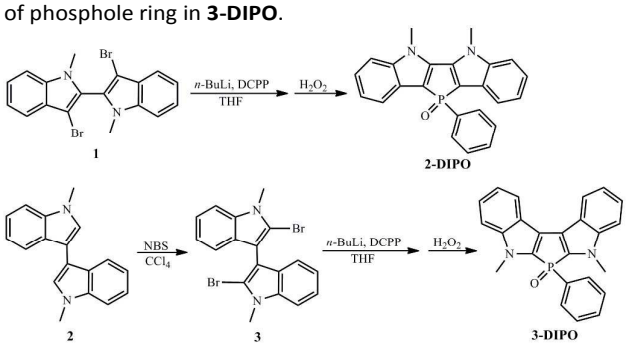

Scheme 1. Synthetic routes for **2-DIPO** and **3-DIPO**.

UV-vis absorption and fluorescence emission spectra in solutions

The UV-vis absorption and fluorescence emission spectra of **2-DIPO** and **3-DIPO** in THF were shown in Figure 1. It was clear that **2-DIPO** gave a strong absorption band at ca. 261 nm with shoulders at ca. 279 nm, 316 m and 331 nm, as well as a broad absorption band at 409 nm. The density functional theory (DFT) calculation at the B3LYP/6-31G level revealed that the absorption at 409 nm for **2-DIPO** was attributed to a HOMO-LUMO transition (π-π* transition, Figure S1). Table S1 showed that the molar absorption coefficient (ε) at 409 nm was 1.2 × 10^4 L·mol^{-1}·cm^{-1}. Compound **3-DIPO** exhibited the strong absorption at ca. 265 nm and weak absorption at ca. 317 nm and 430 nm. The absorption at 430 nm was also due to HOMO-LUMO transition (n-π* transition) confirmed by DFT calculations (Figure S1), but its ε value was as low as 11 L·mol^{-1}·cm^{-1} (Table S1). Additionally, we found that **2-DIPO** and **3-DIPO** gave emission bands at 494 nm and 548 nm, respectively, in THF when excited at 408 nm. The fluorescence quantum yields of **2-DIPO** and **3-DIPO** were 70% and 1.8% in THF, respectively, using 9,10-diphenylanthracene in benzene as reference. Since the emission of **2-DIPO** and **3-DIPO** was originated from π^*-π and π^*-n transitions, respectively, it was understandable that the emission intensity of **2-DIPO** was much higher than **3-DIPO** and a red-shift of the emission of **3-DIPO** compared with **2-DIPO** was observed. Although the emission of **3-DIPO** in THF was weak, its fluorescence quantum yield in solid state reached 0.13, meaning that it was emissive in solid state. It should be noted that the emission band of **3-DIPO** red-shifted to 574 nm in solid state from 548 nm in THF (Figure S2) due to π-π interaction. Similarly, the emission of **2-DIPO** also red-shifted to 530 nm in solid state compared with that in THF, and the solid fluorescence quantum yield was as high as 53%, which made it possible to be used as emitter in OLED.

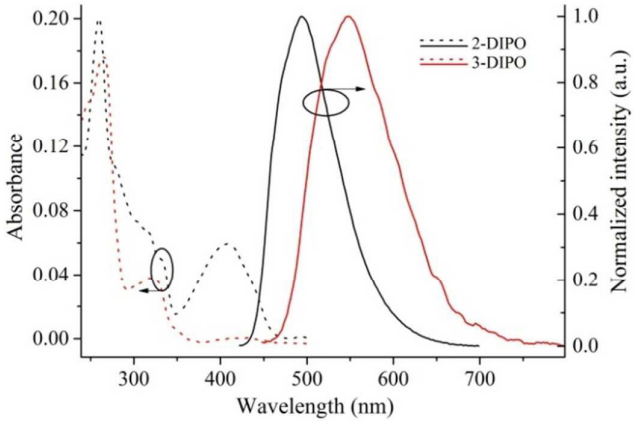

Figure 1. UV-vis absorption and normalized fluorescence emission (λ_{ex} = 408 nm) spectra of **2-DIPO** (5.0 × 10^{-6} M) and **3-DIPO** (5.0 × 10^{-5} M) in THF.

Single crystal structures of 2-DIPO and 3-DIPO

Furthermore, the single crystals of **2-DIPO** and **3-DIPO** were obtained by slow evaporation of the solutions in ethanol/CH_2Cl_2 and methanol/CH_2Cl_2, respectively. As shown in Figure 2, we could find that the indolo-fused phosphole unit in both molecules exhibited planar structure and the benzene

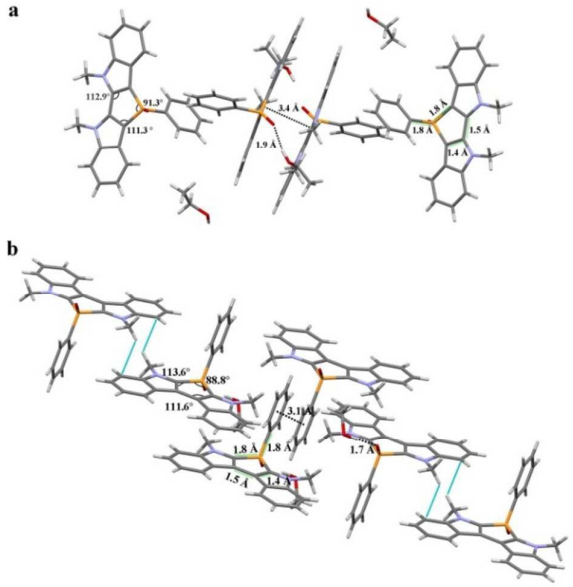

Figure 2. Single crystal structures of **2-DIPO** (a) and **3-DIPO** (b).

Table 1 Electrochemical data and HOMO/LUMO energy levels of **2-DIPO** and **3-DIPO.**

Compound	E_{onset}^{ox} (V)[a]	HOMO[b] (eV)	LUMO[b] (eV)	Eg[c] (eV)	HOMO[d] (eV)	LUMO[d] (eV)	E_g[d] (eV)
2-DIPO	1.19	-5.33	-2.68	2.65	-5.14	-1.54	3.60
3-DIPO	0.90	-5.04	-2.64	2.40	-4.82	-1.28	3.54

[a] E_{onset}^{ox} (V) = onset oxidation potential; [b] $E_{HOMO} = -(E_{onset}^{ox} + 4.15)$ eV; $E_{LUMO} = E_{HOMO} + E_g$; [c] Determined from the onset of the absorption at the lower energy band edge ($Eg = 1240/\lambda_{onset}$); [d] Calculated data.

ring connected with phosphorus atom was almost perpendicular to the indolo-fused phosphole ring. The bond angle of C-P-C in five-membered ring was 91.3°, and the bond lengths of P-C were all 1.8 Å in **2-DIPO** (Figure 2a). In the single crystal of **2-DIPO** the solvent molecules of ethanol were involved. The indolo-fused phosphole units in the adjacent molecules were in a parallel arrangement with a distance of 3.4 Å, and the H-bonding of P=O···H-OC_2H_5 was formed with a distance of 1.9 Å. As shown in Figure 2b, the molecular packing of **3-DIPO** in single crystal was different from that of **2-DIPO**. Benzene rings linked to P atom in the adjacent molecules were arranged in a face to face mode, and the distance between the two benzene rings was 3.1 Å. We also find the H-bonding of P=O···H-OCH_3 with a distance of 1.7 Å in single crystal of **3-DIPO**. Therefore, we deduced that the π-π interaction in the crystal of **2-DIPO** might be stronger than that in the crystal of **3-DIPO**. Meanwhile, we found the formation of C-H···π and the face to face stacking of two benzene rings in the single crystal **3-DIPO**, which led to the higher fluorescence quantum yield of **3-DIPO** in solid state than in solution.[20]

Electrochemical properties and DFT calculations

The electrochemical properties of **2-DIPO** and **3-DIPO** were investigated using cyclic voltammetry with SCE as the reference electrode in CH_2Cl_2. **2-DIPO** showed one reversible oxidation peak and another irreversible oxidation peak with onset potential at around 1.19 V and 1.63 V, respectively. **3-DIPO** showed the similar CV curves with onset potential at ca. 0.90 V and 1.45 V, respectively (Figure S3). We deduced that the appearance of two oxidation peaks for each compound might be originated from the successive oxidation processes of the two indolo rings, and **2-DIPO** exhibited higher oxidation stability. The HOMO energy levels of **2-DIPO** and **3-DIPO** calculated from the oxidation onset potential using the ferrocene calibrated formula of $E_{HOMO} = -(E^{ox}_{onset} + 4.15)$ eV were −5.33 eV, −5.04 eV, respectively. Since the reduction peaks were out of our scan range, the LUMO energy levels of **2-DIPO** and **3-DIPO** were calculated from HOMO energy levels and the absorption band gaps, and were −2.68 eV and −2.64 eV, respectively. Moreover, the molecular orbitals and the optimized configurations of the two compounds were calculated by the B3LYP/6-31G level using the Gaussian 09w program. As shown in Figure 3, the HOMO and LUMO for **2-DIPO** and **3-DIPO** were mainly delocalized through the entire molecules. Based on the calculation results, it was clear that HOMO and LUMO energy levels of **2-DIPO** were lower than those of **3-DIPO** on account of the better conjugated degree of **2-DIPO** than **3-DIPO**.

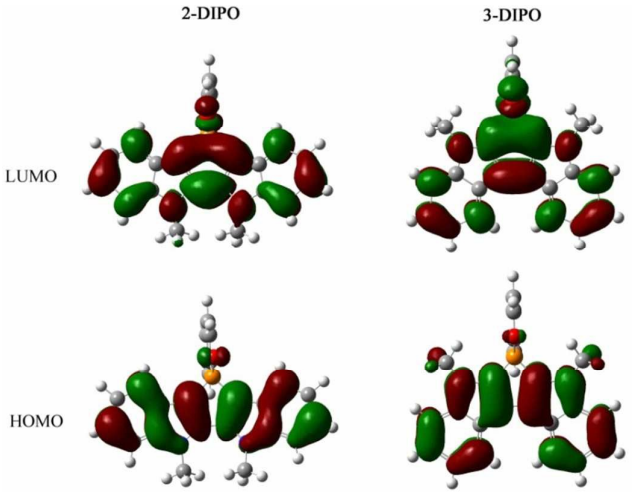

Figure 3 The molecular orbital plots of HOMO and LUMO for **2-DIPO** and **3-DIPO** calculated by the B3LYP/6-31G method using the Gaussian 09w program.

Electroluminescence of 2-DIPO and 3-DIPO

Since **2-DIPO** and **3-DIPO** could emit fluorescence in solid states, we employed them as emitters in OLEDs, and fabricated the OLEDs with the configuration of ITO/NPB (40 nm)/emitter (30 nm)/TPBi (30 nm)/LiF (1.0 nm) /Al (100 nm), in which NPB was N,N'-dinaphtho-1-yl-N,N'-diphenylbenzidine, emitter was **2-DIPO** (named as device A) or **3-DIPO** (named as device B) and TPBi was 1,3,5-tris(N-phenylbenzimidazol-2-yl)benzene. From the electroluminescence spectra (Figure 4), we could find that devices A and B gave the emission located

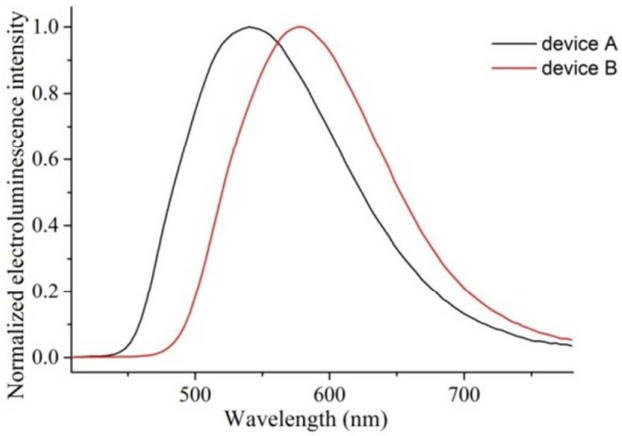

Figure 4. Normalized electroluminescence spectra of devices A and B.

Table 2 EL performance of devices A and B.

Device[a]	λ_{EL}[b] (nm)	Von[c] (V)	L_{max}[d] (cd/m^2)	η_c[e] (cd/A)	η_p[f] (cd/W)
A	540	1.5	2636	1.59	1.35
B	578	2.5	2228	0.22	0.30

[a] Device A and B: ITO/NPB(40nm)/Emitter(30nm)/TPBI(30nm)/LiF(1nm)/Al; [b] Electroluminescence emission peak; [c] Turn-on voltage; [d] Maximum brightness; [e] Maximum current efficiency; [f] Maximum power efficiency.

at 540 nm and 578 nm, respectively, which showed a small red-shift compared with their solid-state photoluminescence. Device A could be turned on at about 1.5 V (1 cd/m^2) and the current density of device A increased with the driving voltage. The brightness of device A increased with the driving voltage in the range of 0-7.5 V, and the brightness reached maximum of 2636 cd/m^2 at the driving voltage of 7.5 V. The maximum current efficiency and maximum power efficiency of device A were 1.59 cd/A and 1.35 cd/W, respectively (Figure S4 and S5). The performance of device B was poorer than device A. In the case of device B, the turned on voltage, maximum brightness, maximum current efficiency and maximum power efficiency were 2.5 V (1 cd/m^2), 2228 cd/m^2 (at 8.0 V), 0.22 cd/A and 0.3 cd/W, respectively (Figure S6 and S7). In order to evaluate the thermal stability of the emitters, DSC and TGA curves for **2-DIPO** and **3-DIPO** were shown in Figure S8. As to **2-DIPO**, the melting point was as high as 334 °C, and the decomposition temperature was above 405 °C. The melting point of **3-DIPO** was at 307 °C and the decomposition temperature was at 348 °C. It indicated that **2-DIPO** and **3-DIPO** exhibited good thermal stabilities, which was a critical issue for device stability. Therefore, the indole-fused phosphole derivatives could be used as emitting materials applied in OLED, and the performance of OLED device based on **2-DIPO** was better than **3-DIPO** on account of its strong emission in solid state. Meanwhile, we found that device A showed better device performance than the non-doped benzothiophene-fused phospholes-based OLED,[16] illustrating that bisindole-fused phospholes were promising emitting materials.

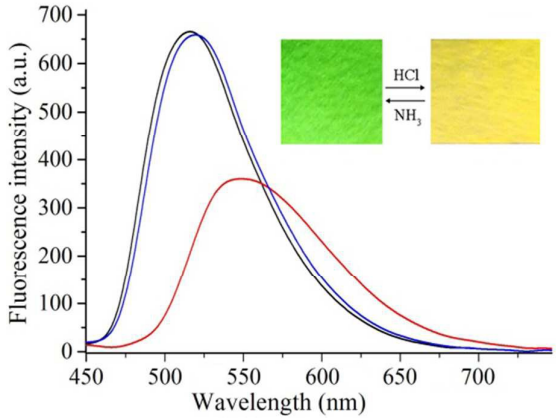

Figure 5. Fluorescence emission spectra of **2-DIPO** in filter paper strip before (black) and after upon exposed to vapors of HCl (red) and NH_3 (blue) in sequence (λ_{ex} = 365 nm). Inset: Photos of filter paper strips based on **2-DIPO** upon exposed with HCl and NH_3 vapors repeatingly under 365 light.

Fluorescence Response towards Acid Vapors

On the other hand, we prepared the filter paper strips containing **2-DIPO** and **3-DIPO**. It was interesting that the emission band of **2-DIPO** located at 517 nm red-shifted to 550 nm, and the emitting color changed from green to yellow upon exposed to HCl vapor (Figure 5). Moreover, the emission could recover to green when the above filter paper strip was exposed to NH_3 vapor. Thus, the filter paper strip based on **2-DIPO** could be used as test paper to sense HCl vapor by naked eyes. Meanwhile, we found that the response reversibility of the test paper was good (Figure S9). However, HCl vapor could not induce any change of the emission of **3-DIPO** in filter paper strip, meaning **3-DIPO** could not sense acid. In order to reveal the different fluorescence sensory behaviors of **2-DIPO** and **3-DIPO** towards gaseous acid, the sensory mechanism should be proposed. In UV-vis absorption spectra titration experiment, trifluoromethanesulfonic acid (TfOH) was selected as analyst due to its good solubility in toluene. As shown in Figure S10, we only found slight red-shift and slight decrease of the intensity of the absorption for **2-DIPO** when 10 equiv. of TfOH was added, illustrating that a weak interaction between **2-DIPO** and TfOH happened and no new species was formed. In ^{1}H NMR titration experiment, slight downfield shifts of H_a and H_b in **2-DIPO** were detected when 1.0 equiv. of TfOH was added (Figure S11), further suggesting the occurrence of weak interaction between **2-DIPO** and TfOH. In this case, we deduced that the formation of H-bonding of CF_3SO_2-O-H···O=P in **2-DIPO** led to the significant changes of the emission of **2-DIPO**. For example, the emission of **2-DIPO** decreased and red-shifted gradually with the increasing of the concentration of TfOH, and it shifted to 550 nm from 497 nm when 20 equiv. of TfOH was added. Additionally, we found that the test paper also exhibited reversible fluorescence response to gaseous strong acids of HBr, HNO_3, trifluoroacetic acid (TFA) and TfOH (Figure S12). However, the weak acid vapors of formic acid and acetic acid could not be detected by the test paper based on **2-DIPO**. To the best of our knowledge, this is the first example of the fluorescence probe based on phosphole derivative to detect acid vapors. Furthermore, similar to the fact that **3-DIPO** could not response towards vapor acid in filter paper strip, the emission of **3-DIPO** could not change upon the addition of TfOH in toluene. We suggested that the P=O in **3-DIPO** was shield by the neighboring groups of N-CH_3 and benzene ring, so that the formation of H-bonding of CF_3SO_2-O-H···O=P in **3-DIPO** would be forbidden.

Conclusions

In summary, we have synthesized two new isomers of phospholes **2-DIPO** and **3-DIPO**, in which indoles were fused with phospholes in different manners. It is found that the OLED using **2-DIPO** as the emitter exhibited moderate performance, but the performance of OLED based on **3-DIPO** was poor due to its weak emission in solid state. Notably, the filter paper strip containing **2-DIPO** could sense gaseous strong acid by naked eyes, and the emitting color of the test paper

changed from green to yellow upon exposed to HCl vapor. This is the first report on the fluorescence probe based on phosphole for detecting acid vapors. **3-DIPO** could not probe acid on account of the steric effect of neighboring groups of O=P to prevent the formation of H-bonding. Therefore, the optoelectronic properties of phosphole derivatives could be tuned by the fused manner of heterocyclic rings to phospholes. It provided a strategy for design novel phospholes with desired functionalities.

Experimental section

General information

The synthetic procedures were performed under N_2 atmosphere. THF was refluxed with Na until the color of solvent turned into atropurpureus using benzophenone as indicator. CH_2Cl_2 and CCl_4 were refluxed with CaH_2 overnight. ^1H NMR, quantitative ^{13}C NMR and ^{31}P NMR spectra were recorded with a Bruker avance III 400 MHz, 100 MHz and 162 MHz, respectively, using $CDCl_3$ and DMSO-d_6 as the solvents. The chemical shifts in ^1H NMR and ^{13}C NMR spectra were reported in parts per million (ppm) relative to $Si(CH_3)_4$ as external standard. The ^{31}P NMR signals were expressed with a positive sign, and the chemical shifts were given in ppm relative to external H_3PO_4 (85 %). Mass spectra were performed on Agilent 1100 MS series and AXIMA CFR MALDI/TOF (matrix assisted laser desorption ionization/time-of-flight) MS (COMPACT). FT-IR spectrum was measured with a Nicolet-360 FT-IR spectrometer by incorporation of sample in KBr disk. DSC measurements were taken by NETZSCH DSC 204 F1 phoenix. TGA measurements were run on a TA Q500 system under N_2 purge with a heating rate of 10 °C/min. UV-vis absorption spectra were determined on a Shimadzu UV-1601PC Spectrophotometer. Fluorescence emission spectra were carried out on a Shimadzu RF-5301 Luminescence Spectrometer. The solid fluorescence quantum yields were measured using Edinburgh Instrument FLS920. Single crystal data were collected with a Rigaku R-AXIS RAPID. Cyclic voltammetry (CV) was performed using a CHI 604C voltammetric analyzer and the measurements were carried out containing 0.1 M Bu_4NBF_4 as a supporting electrolyte. A platinum button was used as a working electrode and a platinum plate as a counter electrode. All potentials were recorded versus SEC as a reference electrode (using ferrocene as an internal standard). The scan rate was maintained at 50 mV s^{-1}. The optimized configurations and the orbital plots of HOMO and LUMO were calculated by the DFT (B3LYP/6-31G) method on the Gaussian 09W software.

The devices were grown on a glass, which was pre-coated with indium tin oxide (ITO) having a sheet resistance equal to 20 Ω cm^{-2}. The ITO glass was routinely cleaned by ultrasonic treatment in detergent solutions, followed by rinsing with acetone, boiling in isopropanol, rinsing in methanol, and then in deionized water. The glass was dried in a vacuum oven between each cleaning step above. To reduce the possibility of electrical shorts on the ITO anode and increase the value of its work function, the ITO substrate was treated using a Plasma Cleaner (PDC-32G-2, 100 W) with the oxygen ambient. Prior to the deposition, all of the organic materials were further purified by the sublimation method. The organic layer was sequentially deposited onto the substrate without breaking vacuum at a pressure of about 10^{-4} Pa. A very thin layer of LiF could enhance electron injection from the aluminum cathode. A shadow mask with 2 × 3 mm^2 openings was used to define the cathodes. The EL spectra, brightness and the current-brightness-voltage characteristics of the devices were measured with a rapid scan system using a spectrophotometer (PR-650, Photo Research) and a computer-controlled, programmable, directcurrent (DC) source (Keithley 2400). Luminance-voltage andcurrent-voltage characteristics were measured at room temperature under an ambient atmosphere. The filter paper strips containing **2-DIPO** and **2-DIPO** were prepared by dipping the filter paper strips in the CH_2Cl_2 solutions, followed by evaporating the solvent naturally.

Synthesis

3,3'-dibromo-1,1'-dimethyl-1H,1'H-2,2'-biindole **1** and 1,1'-dimethyl-1H,1'H-3,3'-biindole **2** were synthesized according to the reported literatures.[12,14,19]

5,6-dimethyl-11-phenyl-5,6-dihydrophospholo[3,2-b:4,5-b']diindole 11-oxide 2-DIPO Under N_2 atmosphere, *n*-BuLi (4.21 mL, 10.52 mmol, 2.5 mol/L in *n*-hexane) was added dropwise to dry THF solution of 3,3'-dibromo-1,1'-dimethyl-1H,1'H-2,2'-biindole (2.0 g, 4.78 mmol) at -78 °C. After stirring for 30 min, $PhPCl_2$ (0.72 mL, 5.26 mmol) was added and the resulting suspension was allowed to warm quickly to room temperature. After stirring for 2 h at room temperature, diluted H_2O_2 (10 mL of 30% H_2O_2 in 40 mL H_2O) was added to the mixture. After stirring for another 2 h, the mixture was slowly poured into saturated solution of $Na_2S_2O_3$ in water. The precipitation was filtered to afford crude product, which was purified by column chromatography using acetone/petroleum (v/v = 1/3) as eluent to afford **2-DIPO** (1.10 g, 60 %) as a bright yellow green solid. Mp. 334.0 °C (obtained from DSC result). ^1H NMR (400 MHz, DMSO-d_6) δ (ppm): 7.76 (dd, J = 13.2, 7.1 Hz, 2H, ArH), 7.67 (d, J = 8.2 Hz, 2H, ArH), 7.53-7.40 (m, 5H, ArH), 7.23 (t, J = 7.3 Hz, 2H, ArH), 7.15 (t, J = 7.4 Hz, 2H, ArH), 4.26 (s, 6H, NCH_3) (See Figure S13). Quantitative ^{13}C NMR (100 MHz, DMSO-d_6) δ (ppm): 143.46, 143.21, 141.97, 141.86, 134.69, 133.57, 132.05, 132.03, 130.87, 130.76, 129.34, 129.22, 126.12, 126.03, 122.94, 122.68, 119.26, 113.73, 112.48, 112.39, 34.54. (See Figure S14). ^{31}P NMR (162 MHz, DMSO-d_6) δ (ppm): 9.00 (See Figure S15). MS, m/z: cal.: 382.1, found: 383.0 $[M+H]^+$ (See Figure S16). IR (KBr, cm^{-1}): 3053, 3011, 2945, 1609, 1570, 1525, 1481, 1460, 1438, 1400, 1364, 1338, 1263, 1204, 1174, 1121, 1106, 1069, 1016, 983, 761, 751, 741, 734, 710, 696, 658, 651, 589, 575, 551, 538, 525, 499, 464, 431.

2,2'-dibromo-1,1'-dimethyl-1H,1'H-3,3'-biindole 3 1,1'-Dimethyl-1H,1'H-3,3'-biindole (2 g, 7.69 mmol) and NBS (1.64 g, 9.22 mmol) were dissolved in dry CCl_4. After refluxed for 5 h, the mixture was cooled to room temperature, and the precipitation was removed by vacuum filtration. The filtrate

was evaporated under reduced pressure and the residual solids were recrystallized in ethyl acetate to afford **3** as a light brown solid. Mp. 110.0-112.0°C. ^{1}H NMR (400 MHz, $CDCl_3$) (ppm): 7.36 (m, 4H, ArH), 7.25 (m, 2H, ArH), 7.08 (m, 2H, ArH), 3.88 (s, 6H, NCH_3) (See Figure S17). IR (KBr, cm^{-1}): 3051, 2937, 2872, 1495, 1463, 1417, 1379, 1352, 1329, 1307, 1228, 1156, 1128, 1097, 1081, 1020, 1011, 913, 802, 742, 583, 550, 428.

5,7-dimethyl-6-phenyl-5,7-dihydrophospholo[2,3-b:5,4-b']diindole 6-oxide 3-DIPO By following the synthetic procedure for **2-DIPO** except using **3** (2.0 g, 4.78 mmol), *n*-BuLi (2.5 mol/L in *n*-hexane, 4.21 ml, 10.52 mmol), $PhPCl_2$ (0.72 ml, 5.26 mmol) and diluted H_2O_2 (10 mL of 30% H_2O_2 in 40 mL H_2O) as reagents. The crude product was purified by column chromatography using acetone/petroleum (v/v = 1/3) as eluent to afford **3-DIPO** (0.86 g, 47 %) as a deep yellow solid. Mp. 308.0 °C (obtained from DSC). ^{1}H NMR (400 MHz, DMSO-d_6) δ (ppm): 8.07 (d, J = 7.9 Hz, 2H, ArH), 7.75 (dd, J = 13.5 Hz, J = 7.5 Hz, 2H, ArH), 7.66 (t, J = 7.1 Hz, 1H, ArH), 7.53 (d, J = 8.2 Hz, 4H, ArH), 7.28 (dt, J = 14.8, J = 7.2 Hz, 4H, ArH), 3.72 (s, 6H, NCH_3) (See Figure S18). Quantitative ^{13}C NMR (100 MHz, DMSO-d_6) δ (ppm): 141.99, 141.91, 133.86, 133.54, 133.52, 132.58, 131.17, 131.05, 130.15, 130.07, 130.03, 128.98, 124.41, 123.07, 122.88, 121.78, 121.56, 121.31, 121.21, 112.20, 32.69. (See Figure S19). ^{31}P NMR (162 MHz, DMSO-d_6) δ (ppm): 6.79 (See Figure S20). MS, m/z: cal.: 382.1, found: 383.1 $[M+H]^+$ (See Figure S21). IR (KBr, cm^{-1}): 3055, 3012, 2934, 2795, 2689, 1611, 1585, 1519, 1497, 1473, 1435, 1405, 1377, 1345, 1309, 1289, 1235, 1202, 1156, 1135, 1098, 1067, 1033, 1011, 933, 914, 826, 811, 780, 736, 714, 697, 646, 637, 606, 584, 568, 549, 496, 449, 439, 425, 406.

Acknowledgements

This work was financially supported by the National Natural Science Foundation of China (21374041) and the Open Project of State Key Laboratory of Supramolecular Structure and Materials (SKLSSM2015014).

Notes and references

1 (a) F. J. M. Hoeben, P. Jonkheijm, E. W. Meijer, A. P. H. J. Schenning. *Chem. Rev*. 2005, **105**, 1491-1546; (b) C. L. Wang, H. L. Dong, W. P. Hu, Y. Q. Liu, D. B. Zhu. *Chem. Rev*. 2012, **112**, 2208-2267; (c) J. Roncali. *Chem. Soc. Rev*., 2005, **34**, 483-495; (d) L. Zang, Y. K. Che, J. S. Moore. *Acc. Chem. Res*. 2008, **41**, 1596-1608; (e) S. L. Xu, N. Ai, J. Zheng, N. Zhao, Z. G. Lan, L. R. Wen. *RSC Adv.*, 2015, **5**, 8340-8344; (f) Y. S. Guan, Y. K. Qin, Y. H. Sun, C. Wang, W. Xu, D. B. Zhu. *Chem. Commun*., 2015, **51**, 12182-12184.

2 (a) F. S. Kim, G. Q. Ren, S. A. Jenekhe. *Chem. Mater*. 2011, **23**, 682-732; (b) P. A. Korevaar, T. F. A. D. Greef, E. W. Meijer. *Chem. Mater*. 2014, **26**, 576-586; (c) V. Coropceanu, J. Cornil, D. A. da Silva Filho, Y. Olivier, R. Silbey, J. L. Brédas. *Chem. Rev*. 2007, **107**, 926-952; (d) L. Ding, S. C. Dong, Z. Q. Jiang, H. Chen, L. S. Liao. *Adv. Funct. Mater*. 2015, **25**, 645-650; (e) S. T. Zhang, L. Yao, Q. M. Peng, W. J. Li, Y. Y. Pan, R. Xiao, Y. Gao, C. Gu, Z. M. Wang, P. Lu, F. Li, S. J. Su, B. Yang, Y. G. Ma. *Adv. Funct. Mater*. 2015, **25**, 1755-1762.

3 (a) T. Baumgartner, R. Réau. *Chem. Rev*. 2006, **106**, 4681-4727; (b) D. Joly, D. Tondelier, V. Deborde, B. Geffroy, M. Hissler, R. Réau. *New J. Chem*. 2010, **34**, 1603-1611; (c) H. C. Su, O. Fadhel, C. J. Yang, T. Y. Cho, C. Fave, M. Hissler, C. C. Wu, R. Réau. *J. Am. Chem. Soc*. 2006, **128**, 983-995.

4 C. Fave, T. Y. Cho, M. Hissler, C. W. Chen, T. Y. Luh, C. C. Wu, R. Réau. *J. Am. Chem. Soc*. 2003, **125**, 9254-9255.

5 (a) S. Y. Cai, G. J. Tian; X. Li, J. H. Su, H. Tian. *J. Mater. Chem. A*., 2013, **1**, 11295-11305; (b) J. Yu, J. Luo, Q. Chen, K. He, F. Meng, X. Deng, Y. Wang, H. Tan, H. Jiang, W. Zhu. *Tetrahedron*, 2014, **70**, 1246-1251.

6 (a) P. Gong, P. C. Xue, C. Qian, Z. Q. Zhang, R. Lu. *Org. Biomol. Chem.*, 2014, **12**, 6134-6144; (b) P. Gong, J. B. Sun, P. C. Xue, C. Qian, Z. Q. Zhang, J. B. Sun, R. Lu. *Dyes Pigments*, 2015, **118**, 27-36; (c) G. H. Hong, J. B. Sun, C. Qian, P. C. Xue, P. Gong, Z. Q. Zhang; R. Lu. *J. Mater. Chem. C.*, 2015, **3**, 2371-2379.

7 J. Peng, J. B. Sun, P. Gong, P. C. Xue, Z. Q. Zhang, G. H. Zhang, R. Lu. *Chem. Asian J.* 2015, **10**, 1717-1724.

8 (a) G. M. Nie, L. J. Zhou, Q. F. Guo, S. S. Zhang. *Electrochem. Commun*. 2010, **12**, 160-163; (b) Y. J. Na, W. Song, J. Y. Lee, S. H. Hwang. *Org. Electron*. 2015, **22**, 92-97.

9 (a) C. W. Lee, J. Y. Lee. *Adv. Mater*. 2013, **25**, 5450-5454; (b) M. S. Park, D. H. Choi, B. S. Lee, J. Y. Lee. *J. Mater. Chem.* 2012, **22**, 3099-3104.

10 (a) L. Zou, B. Yan, D. Pan, Z. Tan, X. Bao. *Spectrochim. Acta, Part A*, 2015, **148**, 78-84; (b) F. M. Pfeffer, K. F. Lim; K. J. Sedgwick. *Org. Biomol. Chem*. 2007, **5**, 1795-1799.

11 (a) K. J. Chang, D. Moon, M. S. Lah, K. S. Jeong. *Angew. Chem., Int. Ed*. 2005, **117,** 8140-8143.; (b) J. L. Sessler, D. G. Cho, V. Lynch. *J. Am. Chem. Soc*. 2006, **128**, 16518-16519.

12 M. Barboiu. *Eur. J. Inorg. Chem*. 2015, 1112-1125.

13 T. Qi, W. Qiu, Y. Liu, H. Zhang, X. Gao, Y. Liu, K. Lu, C. Y. Du, G. Yu, D. B. Zhu. *J. Org. Chem.* 2008, **73**, 4638-4643.

14 M. Stolar, J. Borau-Garcia, M. Toonen, T. Baumgartner. *J. Am. Chem. Soc.* 2015, **137**, 3366-3371.

15 S. Furukawa, S. Haga, J. Kobayashi, T. Kawashima. *Org. Lett.* 2014, **16**, 3228-3231.

16 H. Chen, W. Delaunay, J. Li, Z. Y. Wang, P. A. Bouit, D. Tondelier, B. Geffroy, F. Mathey, Z. Duan, R. Réau, M. Hissler. *Org. Lett*. 2013, **15**, 330-333.

17 Y. Dienes, M. Eggenstein, T. Kárpáti, T. C. Sutherland, L. Nyulászi, T. Baumgartner. *Chem. Eur. J*. 2008, **14**, 9878-9889.

18 Y. Xu, Z. Wang, Z. Gan, Q. Xi, Z. Duan, F. Mathey. *Org. Lett*. 2015, **17**, 1732-1734.

19 P. W. Zhang, R. Y. Liu, J. M. Cook. *Tetrahedron Lett*. 1995, **36**, 3103-3106.

20 (a) Y. Hong, J. W. Y. Lam, B. Z. Tang. *Chem. Commun.* 2009, 4332-4353; (b) P. C. Xue, B. Q. Yao, J. B. Sun, Z. Q. Zhang, R. Lu. *Chem. Commun.* 2014, **50**, 10284-10286; (c) P. C. Xue, R. Lu, P. Zhang, J. H. Jia, Q. X. Xu, T. R. Zhang, M. Takafuji, H. Ihara. *Langmuir* 2013, **29**, 417-425; (d) X. L. Liu, D. F. Xu, R. Lu, B. Li, C. Qian, P. C. Xue, X. F. Zhang, H. P. Zhou. *Chem. Eur. J.* 2011, **17**, 1660-1669; (e) P. Chen, R. Lu, P. C. Xue, T. H. Xu, G. J. Chen, Y. Y. Zhao. *Langmuir*, 2009, **25**, 8395-8399; (f) Y. Bao, R. Lu, M. Jin, P. C. Xue, C. H. Tan, G. F. Liu, Y. Y. Zhao. *Chem. Eur. J.* 2006, **12**, 3287-3294.